Growth and Transport Properties of [Rare Earth]TiO3/SrTiO3 Interfaces

Lebedev, N.

Cover Page

Universiteit Leiden

The handle http://hdl.handle.net/1887/138477 holds various files of this Leiden University dissertation.

Author: Lebedev, N.
Title: Growth and Transport Properties of [Rare Earth]TiO3/SrTiO3 Interfaces
Issue Date: 2020-12-01

2

Experimental Methods

2.1. Introduction

This chapter describes the experimental methods used in this work. The first section describes the thin film fabrication process, namely the preparation of a TiO_2-terminated $SrTiO_3$ surface, the growth of the films by Pulsed Laser Deposition and the use of Reflection High Energy Electron Diffraction (RHEED). The second section is dedicated to the back gate experiments performed in the Leiden measurement platform (a PPMS from Quantum Design), and in particular to the insert which was designed and built for these experiments. The last section briefly list the techniques which have been used by our collaborators.

2.2. Sample preparation

2.2.1. Termination of $SrTiO_3$

The $SrTiO_3$ substrates used in this work have a (001) orientation with 0.1-0.3° miscut angles and were purchased from CrysTec GmbH. In order to create a 2DEL at the interface of STO(001) and a polar oxide, TiO_2-termination is required [18]. The method used in this work is the somewhat altered procedure proposed by Koster *et al.* [195]:

1) (Optional) cleaning with lens paper with isopropanol;

2) Sonication for 5 min in acetone;

3) Sonication for 5 min in ethanol;

4) Sonication for 30 min in ultrapure water;

5) Etching for 30 sec in buffered HF;

6) Annealing for 1 hour for a miscut angle >0.2° and 1.5 hour for a miscut angle <0.2° at temperature 950-980 °C in a tube furnace at 100-150 ml/min O_2 flow.

The first three steps are needed to remove surface contaminants on as-received substrates. The fourth is necessary to create $Sr(OH)_2$ [195] in order to ensure removal of SrO. After etching the obtained surface will be TiO_2-terminated, but annealing at 950 °C in oxygen is required to obtain a recrystallized surface [195]. An Atomic Force Microscopy (AFM) scan of the resulting surface is shown in Fig. 2.1a. The characteristic step pattern indicates TiO_2-termination [195, 196]. The
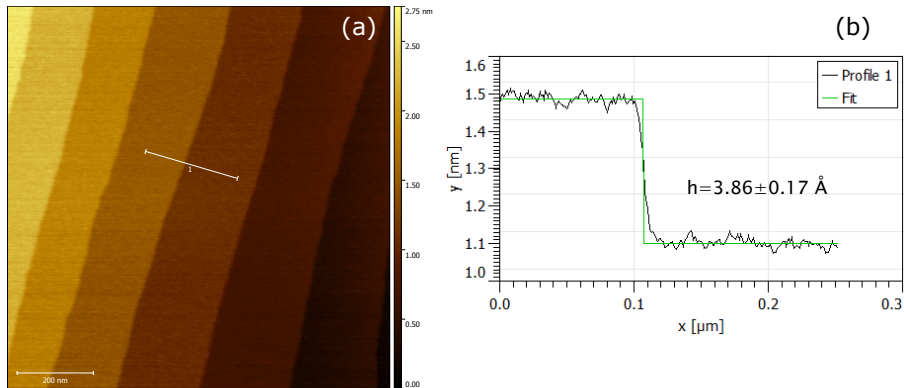
Figure 2.1: (a) AFM image of SrTiO$_3$ (001) surface after going through the single termination process and (b) line profile along the line shown in (a) with the fit to determine the step height.

height of a typical step is obtained from a fitted line profile, presented in Fig. 2.1b. The difference between the obtained value of 3.86 Å and the expected value of 3.90 Å is within the uncertainty of the fit.

2.2.2. Pulsed Laser Deposition

After the substrates were terminated, films were grown by the Pulsed Laser Deposition (PLD) technique, using the PLD-RHEED system at the University of Twente. PLD is a deposition technique which utilized high energy UV laser pulses to produce a plasma from a target material. PLD has some important advantages over other deposition techniques for the presented work such as stoichiometric transfer of material (under optimal conditions), the possibility of reactive deposition in an ambient gas, and a high kinetic energy of ablated species helping to obtain single crystalline films. Among the relevant disadvantages are a nonuniform film thickness distribution and crystallographic defects due to the bombardment of the film by high kinetic energy particles [197, 198].

The PLD-RHEED system is equipped with a UV KrF excimer laser (Laser Plasma Physik LPX Pro 210) producing at wavelength of $\lambda = 248$ nm. A set of mirrors directs the laser through a focusing lens and an optical window into a vacuum chamber to a target. The vacuum chamber has a base pressure of 3×10^{-7} mbar. At a certain position depending on the required fluency and the laser spot parameters a metal

mask (a rectangular one in this work) was mounted to select the most uniform part of the laser spot. To control the fluency, the laser voltage and an optical attenuator were used, as well as masks with different area. An energy meter was used to optimize the energy before and after the lens to ensure the correct fluency. The pulse frequency of the laser was fixed at 1 Hz.

A laser pulse, typically with an energy of a few J/cm^2, leads to rapid heating of the target material, which start to evaporate [197]. The light absorption in the vapor keeps increasing until it breaks down and a plasma forms. Further absorption heats and accelerates the plasma. In the high-density region near the target plasma particles undergo collisions leading to expansion perpendicular to the target surface. During deposition, the laser scans the target in a horizontal direction to ensure uniformity. The deposition can be performed in O_2, Ar or in a mixed atmosphere. In Ar (or any other inert gas) there will be a shock front due to collisions between the plasma and Ar atoms. In O_2 (or any reactive gas), besides the shock front, O_2 will chemically react, leading to formation of oxide molecules (if gas is O_2). The gas pressure range (either Ar or O_2) used in this work is $5 \times 10^{-5} - 1 \times 10^{-3}$ mbar. The plasma plume is directed towards the substrate, which is glued to a heater by Leitsilber 200 silver paint. Before the deposition the heater temperature is ramped up to the deposition temperature (usually in 650-900 °C range), at the deposition pressure [197]. The system does not have the possibility to rotate substrate during film growth, which can lead to a non-uniform film thickness at low pressures. Proper growth can be very sensitive to even small changes in the laser parameters such as fluency and spot size. The parameters for this can be found in the relevant chapters.

2.2.3. Reflection High-Energy Electron Diffraction

The PLD-RHEED system is equipped with a Reflection High-Energy Electron Diffraction (RHEED) setup. An electron beam is directed at a grazing angle ($\geqslant 3°$) with respect to the substrate surface and produces a diffraction pattern on a phosphorous display. A CCD camera collects images of the patterns and measures its intensities [199]. RHEED allows *in-situ* real time characterization of the film growth process. First of all, it gives information of the growth regime by monitoring the intensities of diffracted spots, in particular the specular beam. In case of step-flow growth the intensity does not change significantly because a layer start to grow from edges of the substrate steps and the overall surface morphology is

unchanged. In case of 3D growth, islands are formed, but due to low mobility of deposited particles, they do not form a complete layer before islands on the next layer start to form. The surface becomes rough very quickly, the the intensity decreases, and diffraction spot positions become independent of the angle of incidence. In case of amorphous growth, the intensity also decreases, but now also the diffraction pattern disappears. In case of layer-by-layer growth, 2D islands are formed and merge, so that after one deposited layer or unit cell, the surface is flat again. That growth mode produces (specular beam) intensity oscillations, as for instance shown in Fig. 2.2. They can be used to count the number of deposited unit cells in real time [195].

The RHEED pattern also allows to characterize the quality of the films grown. As an example, the pattern of a single crystal STO substrate at room temperature before deposition is presented in Fig. 2.3a. The pattern above the shadow line corresponds to STO. The diagonal so-called Kikuchi lines are characteristic of high crystallinity also into the depth of the crystal. The bottom spot is from the direct beam. Amorphous film growth, in this case of ELTO (sample #3), resulted in the cloudy pattern shown in Fig. 2.3b. The pattern after growing GTO (sample #12) indicates 2D growth (Fig. 2.3c), while 3D growth with some signatures of amorphization was observed after preparation of ELTO/STO sample #12 (Fig. 2.3d).
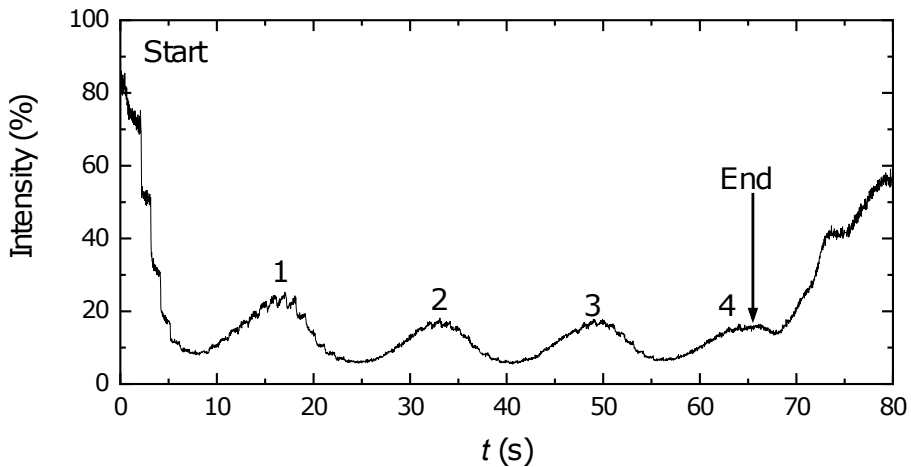
Figure 2.2: The RHEED oscillations of ELTO/STO-13.
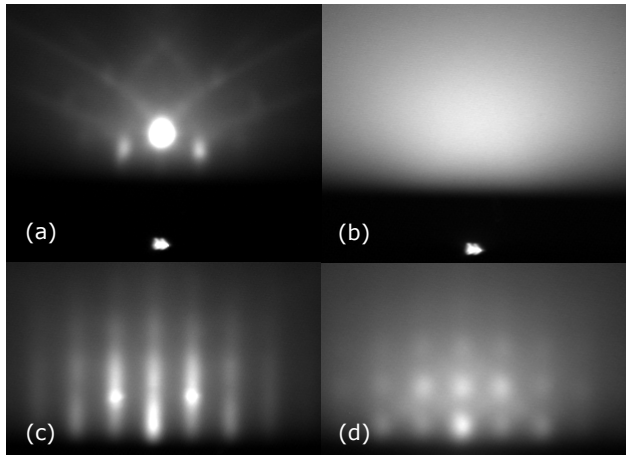
Figure 2.3: The RHEED pattern of (a) SrTiO$_3$ surface at room temperature before deposition and (b) ELTO/STO-3, (c) LGAO/GLTAO/STO-12, (d) ELTO/STO-12 after deposition.

2.3. Back gating experiments in the PPMS

In this section back gating experiments, including measurements in the so-called van der Pauw geometry are described. For a description of the physical mechanism of the back gating see Section 1.

2.3.1. Insert

In order to perform back gate experiments in our measurement platform, a PPMS from Quantum Design, a special back gate insert with proper grounding for the gating experiments was designed and built. It is shown in Fig. 2.4. Because of a tradeoff between reliability, simplicity of use, time costs and required characteristics the temperature range for use of the insert is 350 K to 3 K, instead of the 400 K - 2 K range which can be supported by the PPMS. The insert was based on a 'multifunctional probe for' the PPMS, but significant changes have been made on the original design. A few parts were left from the original probe, in particular:

1) The cylindrical probe head;

2) The O-ring on the top, which provide a vacuum-tight connection when the insert is installed in the PPMS;

3) The stainless steel tube;

4) Radiation baffles outside and inside of the tube (only the outside ones can be seen in Fig. 2.4), to minimize heat radiation between parts at 300 K and 3 K;

5) The mechanical part of the PPMS puck assembly to ensure a fixed position, when installed in the PPMS;

6) The body for mechanical attachment at the bottom of the probe.

The following parts were replaced or added:

1) The factory-made top of the head was replaced by a homemade one with a vacuum Jaeger connector (not shown in Fig. 2.4), which allows direct access to wiring without using the standard PPMS wires;
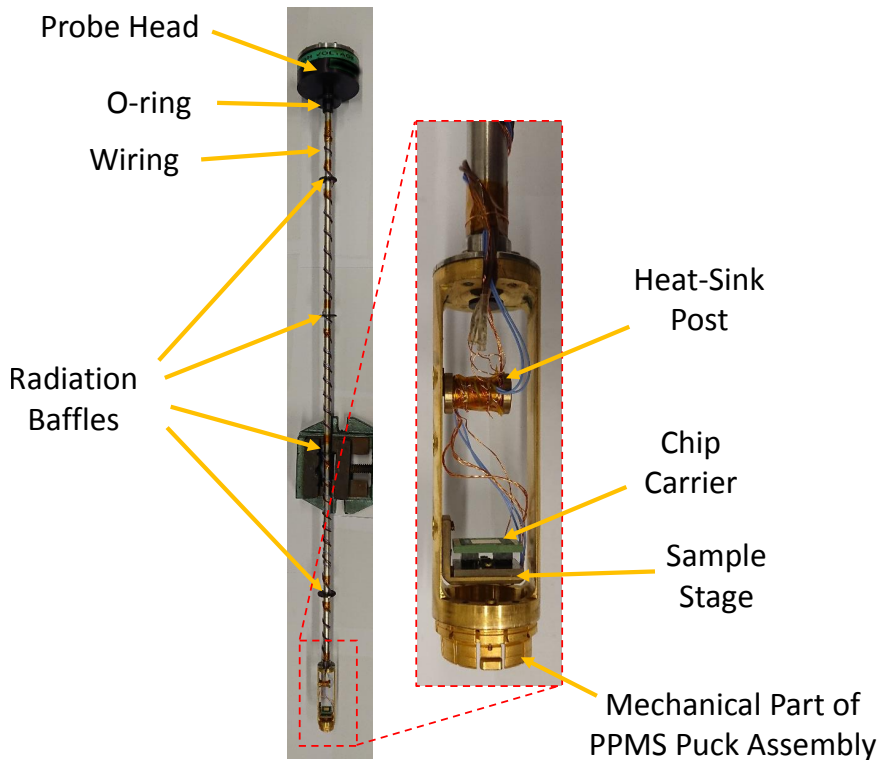
Figure 2.4: The photo of the back gate voltage PPMS insert.
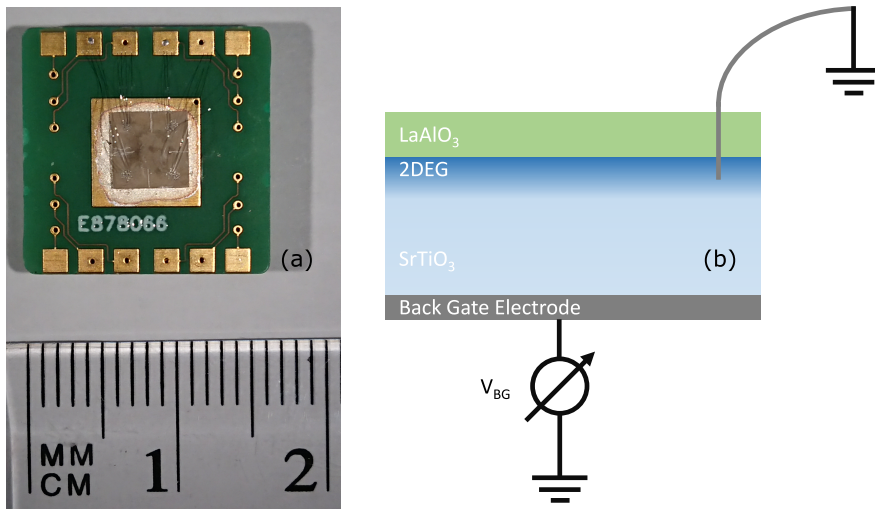
Figure 2.5: (a) Photo of a chip carrier with a mounted sample. (b) The electrical layout of the back gate voltage experiments.

2) Old wiring was removed and replaced by a new set of cables:

   (a) One twisted pair and one twisted quad of copper wires for measurements;

   (b) Two stainless steel coaxial cables with Teflon insulation for a thermometer;

   (c) One twisted pair of copper wires with Teflon insulation for back gate and ground connections;

3) A heat-sink post to thermally anchor the wiring;

4) A sample stage, which can be oriented parallel and perpendicular to the magnetic field direction;

5) The chip carriers, which have plug-in connectors for the sample stage;

6) The thermometer clamped under the chip carrier to the sample stage.

The chip carrier was also designed in-house. In Fig. 2.5a the chip carrier with a mounted sample is shown. The sample is glued by Leitsilber 200 silver paint to the central back gate electrode and connected by wires which were wirebonded from the sample to the contact pads. In Fig. 2.5b the electrical layout of the back gate experiment is presented. Most of the measurements were performed with an

AC current of about $0.1 - 1$ μA at frequencies $15 - 150$ Hz using a lock-in amplifier SR-830. To increase the lock-in input impedance, a pre-amplifier SR-550 was used. Zener (diode) clamps were connected to the lock-in inputs for protection from voltage overload. Special software in Python was written to control the measurement equipment and the MultiVu program which controls the PPMS.

2.3.2. Van der Pauw measurements

Most of results obtained in this thesis are on samples measured in the van der Pauw (VDP) geometry [200, 201]. In this geometry, four contacts are placed along the perimeter of a sample. This is not always convenient in case of oxide structures, because low pressure deposition conditions can lead to a non-uniform distribution of the material. Moreover, in order to avoid leakage currents, the sample edges have to be polished to remove silver paint remnants after PLD. This process may lead to damaged edges. To ensure measurements through the central and presumably homogeneous part of the sample, in some of them scratches were made by a diamond knife in the middle of the center of each edge, in order to block currents along the sides and only probe the central part. To measure the sheet resistance, voltage probes were always connected to the edge opposite to the edge with current leads. For the Hall resistance, the voltage probes were connected to one diagonal and the current probes to another one. Switching between the different combinations was made with a programmable relay box.

Below, the calculation of the sheet resistance and the Hall resistance from the measured set of resistances will be explained, but first some definitions need to be introduced. For the contacts named as in Fig. 2.6, $R_{ij,kl}$ is defined as follows:

$$R_{ij,kl} = \frac{V_{kl}}{I_{ij}}, \tag{2.1}$$

where V_{kl} is the voltage measured between contacts l and k, with contact l connected to $V+$ and k to $V-$; I_{ij} is the current between contacts i, connected to $I+$, and j, connected to $I-$. Two resistance-type quantities can be calculated by the following equations:

$$R^{Ho}(B) = \frac{R_{AB,CD} + R_{BA,DC} + R_{DC,BA} + R_{CD,AB}}{4}, \tag{2.2}$$

$$R^{Ve}(B) = \frac{R_{AD,CB} + R_{DA,BC} + R_{CB,AD} + R_{BC,DA}}{4}, \tag{2.3}$$

where $R^{Ho}(B)$ and $R^{Ve}(B)$ are resistances corresponding to horizontal and vertical voltages at the applied magnetic field B. Then the van der Pauw equation has to be
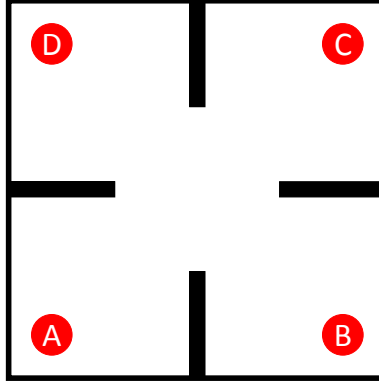
Figure 2.6: The scheme of Van der Pauw geometry. Black lines indicate scratches made to probe the central part of the sample. Letters denote the contacts.

solved:

$$\exp\left(-\pi R^{Ve}/R_S^{meas}\right) + \exp\left(-\pi R^{Ho}/R_S^{meas}\right) = 1, \tag{2.4}$$

where R_S^{meas} is the sought-for sheet resistance. Although this equation cannot be solved analytically, it can be solved numerically, for example by a Newton-Raphson method, which was used in this work. The Hall resistance can be obtained from the following formula:

$$R_{xy}^{meas}(B) = \frac{R_{AC,DB} + R_{CA,BD} + R_{BD,AC} + R_{DB,CA}}{4}. \tag{2.5}$$

After that, the data still need to be (anti-)symmetrized:

$$R_S(B) = \frac{R_S^{meas}(B) + R_S^{meas}(-B)}{2}, \tag{2.6}$$

$$R_{xy}(B) = \frac{R_{xy}^{meas}(B) - R_{xy}^{meas}(-B)}{2}, \tag{2.7}$$

This implicitly means that the measurement needs to be done both for positive and negative field directions. However, to reduce measurement time and to avoid complex electrostatic behavior in not highly conducting samples due to the switch of ground contacts for a next measurement configuration, the number of measured resistances can be limited to two, $R^{Ho}(B) = R_{BA,DC}$ and $R^{Ve}(B) = R_{DA,BC}$, for the sheet resistance, which is later used to solve the VDP equation, and one for the Hall effect measurement $R_{xy}^{meas}(B) = R_{CA,BD}$.

2.4. Additional experimental techniques

This work would not be possible without data obtained by collaborators using their own specialized techniques. Most of PLD targets used for this project were commercially purchased, but the $EuTiO_3$ and $Eu_{0.9}La_{0.1}TiO_3$ targets were pressed and sintered at the University of Amsterdam. The crystal structure of the samples was analyzed by Scanning Transmission Electron Microscopy (STEM), and Electron Energy Loss Spectroscopy (EELS) were used to obtain information about chemical composition. These STEM and EELS experiments were performed at the University of Antwerp. Scanning SQUID microscopy at the University of Twente was used to obtain information about the magnetic state of some films. Low temperature measurements, below 1 K, were performed in a Triton^{TM} dilution fridge from Oxford instruments, also at the University of Twente.